Engineering Solid Mechanics 12 (2024) 165-176

Contents lists available at GrowingScience

Engineering Solid Mechanics

homepage: www.GrowingScience.com/esm

High-pressure torsion effect on microstructural and hardness properties of Magnesium with Silicon Carbide nanoparticles

R.T. Tebeta[a], N. Madushele[b], H.M. Ngwangwa[a*], D.M. Madyira[b] and Z. Wang[a,c,d]

[a]*Department of Mechanical Engineering, College of Science, Engineering and Technology, School of Engineering, University of South Africa, Florida, 1710, Johannesburg, South Africa*
[b]*Mechanical Engineering Science Department, Faculty of Engineering and Built Environment, University of Johannesburg, 2006, Johannesburg, South Africa*
[c]*Centre for Advanced Laser Manufacturing (CALM), Shandong University of Technology, Zibo 255000, PR China*
[d]*School of Mechanical Engineering, Shandong University of Technology, Zibo 255000, PR China*

ARTICLEINFO

Article history:
Received 23 July 2023
Accepted 4 October 2023
Available online
4 October 2023

Keywords:
Microhardness
High-Pressure Torsion
Magnesium with Silicon Carbide
Microstructural Characterisation
Grain size

ABSTRACT

Without a doubt, lightweight materials of high strength are in high demand in the automotive, aerospace, biomedical, and other industries that require such materials. Processing or manufacturing such materials has been a vital topic in contemporary research, as well as material development in the industry. A possible solution for the processing of lightweight materials of high strength is to target lightweight materials by nature such as magnesium and improve their mechanical properties such as stiffness, strength, and hardness. The aforementioned properties are sometimes achieved by processing soft and light materials through High-Pressure Torsion. In this work, Magnesium with Silicon Carbide nanoparticles (Mg-SiC) was strengthened and hardened through the High-Pressure Torsion (HPT) processing technique. The samples were compressed with a pressure of 6.0 GPa and twisted at the rotating speed of 1 rpm with varying numbers of turns N = 0, N = 1, N = 5 and N = 10 at a temperature of 23°C. The processed samples were prepared for the experimental investigation of microstructural characterization and hardness test examinations. Microstructural results showed that grain refinements of material can be achieved through HPT processing methods, which reduced the average grain sizes of unprocessed (N = 0) Mg alloy samples from 149.9 µm to 27.1 µm after processing ten turns. However, hardness test results do not indicate any significant improvement after one HPT processing turn although homogeneity is attained at five processing turns within the nanocomposites.

1. Introduction

Over the years with an ever-increasing demand for economic use of the scarce energy resources and ever-stricter control over greenhouse gas emissions, industry is searching for new and advanced materials as alternatives to conventional materials (Gupta & Sharon, 2011). Magnesium (Mg) offers such an alternative with its high energy efficiency coupled with high specific mechanical properties. As a structural material Mg is the lightest with a density of 1.74 g/cm^3 making it 33% lighter than aluminium and 75% lighter than steel (Gupta & Sharon, 2011; Ross, 2013). When compared to other common structural metals (i.e. steel, Aluminum and Titanium), some Mg alloys (such as AZ61) are reported to yield the highest specific stiffness and rank second in specific strength only to Titanium sheet. As orthopaedic materials, Mg alloys have greater fracture toughness than hydroxyapatite with elastic modulus and compressive strength very close to that of natural bone (Gupta & Sharon, 2011; Ross, 2013). Mg and its alloys also have good biocompatibility and biodegradability. However, the biggest challenges with Mg and its alloys lie in their processing and corrosion resistance. Due to its low electrode potential, Mg tends

* Corresponding author. Tel.: +27(0)11 471 2079
E-mail addresses: ngwanhm@unisa.ac.za (H.M. Ngwangwa)

ISSN 2291-8752 (Online) - ISSN 2291-8744 (Print)

doi: 10.5267/j.esm.2023.10.001

to be anodic to most metals when exposed to moist conditions, and its hexagonal close-packed crystal structure with limited slip systems makes it very hard to be formed without inducing microcracking along the grain boundaries (Dziubińska et al., 2016; Gupta & Sharon, 2011; Ross, 2013). Therefore, considering all the opportunities that Mg and its alloys offer to industry, there is a lot of research aimed at improving their formability at all temperatures as well as their resistance to corrosion. One of the methods that has been widely used in industry to improve material formability is severe plastic deformation (SPD). SPD methods have been widely investigated and acclaimed to attain material formability and grain refinement as well as overcoming a number of other well-known problems such as residual porosity and sample impurities (Valiev et al., 2000; Zhilyaev & Langdon, 2008; Zhu et al., 2004). Unlike other SPD methods, which have been reported to induce microcracking in Mg, HPT has been shown to induce grain refinement with greater fractions of volumes with high angles of misorientation without microcracking even when processed at low temperatures (Alsubaie et al., 2022; Figueiredo & Langdon, 2019). This is attributed to the application of the hydrostatic pressure in the HPT process (Alsubaie et al., 2022; Figueiredo & Langdon, 2019). Harai et al. (2008) investigated the mechanical properties of AZ61 Mg alloy processed with High-Pressure Torsion (HPT) at the temperature of 423 K. Their tensile test results showed that the maximum of 620% superplastic elongation could be achieved at the temperature of 473 K. This was slightly bettered by (Alsubaie et al., 2022) who achieved a superplastic elongation of 645% in AZ80 at a temperature 573 K. Harai et al. (2008) further conducted the microstructural examination that showed an excellent grain refinement on AZ61 magnesium alloy samples with the average sizes of 0.22 μm and 0.11 μm. Alil et al. (Alil et al., 2014) studied the effect of the accumulative roll bonding (ARB) process on the microstructural and mechanical properties of annealed AA5083 Al-Mg alloy sheets. Their results showed that the microstructures of AA5083 Al-Mg alloy sheets were refined, and their mechanical properties improved significantly. Their tensile strength and hardness results proved to be two or three times better than the unprocessed materials when processed up to 6 ARB cycles at room temperature. Shirooyeh et al. (2014) investigated mechanical characteristics and microstructural evolution of grade 2 commercially pure Titanium processed with HPT at room temperature. The Vickers microhardness test results demonstrated homogeneous hardness properties of Titanium samples after five or more processing turns. Moreover, their microstructural results achieved significant grain refinements on Titanium samples with the average grain size reduction from 45 μm for unprocessed samples to 150 nm after ten turns of the HPT process. Rosalie and Pauw (2014) examined the characteristics of the precipitates formed in HPT treated Mg Zn 3.4% alloy. Their results showed that the HPT process resulted in fine-scale precipitation without post-deformation heat treatment. At the same time some studies have shown that Zn based Mg alloys retained corrosion-prone properties after the HPT process making them suitable as biodegradable materials (Brunner et al., 2021; Holweg et al., 2020; Ibrahim et al., 2017; Mizelli-Ojdanic et al., 2021). Alsubaie et al. (2016) examined microstructural and hardness properties of magnesium alloy AZ80 processed by HPT technique. Their microstructural results showed that AZ80 specimens with the initial average grain sizes of 25 μm were improved to 200 nm after being processed with HPT up to 5 and 10 turns at the imposed pressure of 6.0 GPa. The Vickers microhardness (HV) results showed an increase from 63 to 120 at the same processing parameters.

The existing literature shows that there is an extensive scope of research to undertake especially with respect to Mg alloys due to their relative difficulty in their processing because of the limited slip system within their crystal microstructure. However, this paper studies the effect of HPT processing technique on the microstructural and hardness properties of Mg-SiC processed at the imposed pressure of 6.0 GPa with a rotational speed of 1 rpm, and at the temperature of 23 ^{0}C for various processing turns: N = 0, N = 1, N = 5, and N = 10. This nanocomposite has stable warpage, excellent high thermal conductivity and heat dissipation. It is mainly used in power modules for electric railway, industrial machinery and automotive. Mg-SiC is reported to have superior thermal conductivity and deformation at elongated durations to the conventional material Aluminum with Silicon Carbide (Al-SiC). In this paper we only examine the evolution of its microstructure and hardness under HPT processing.

2. Equivalent Strain and Microhardness Calculations

Consider that the test specimen thickness is represented as h which is independent of the rotation angle θ, and that the radius of the specimen is represented by *r*. The total shear strain γ in the specimen is given by (Xu et al., 2008; Zhilyaev et al., 2007; Zhilyaev & Langdon, 2008).

$$\gamma = \frac{\theta.r}{h} = \frac{2\pi N.r}{h} \tag{1}$$

where N is the number of twist rotations. Thus, the equivalent Von Mises strain for small strains is estimated by

$$\varepsilon = \frac{\gamma}{\sqrt{3}} \tag{2}$$

In large imposed shear strains where $\gamma \gg 0.8$, the equivalent Von Mises strain ε is given by Zhilyaev et al. (2007).

$$\varepsilon = \frac{2}{\sqrt{3}} \ell n \left(\sqrt{1 + \frac{\gamma^2}{4}} + \frac{\gamma}{2} \right) \tag{3}$$

If we incorporate the decrease in the thickness of the HPT processed disk as a consequence of the applied hydrostatic pressure by the top anvil, the equivalent Von Mises is expressed as (Xu et al., 2008; Zhilyaev et al., 2007).

$$\varepsilon = \ell n \left(\sqrt{1 + \left(\frac{\theta . r}{h} \right)^2} + \ell n \left(\frac{h_0}{h} \right) \right) \tag{4}$$

where h_o and h denote the initial and final thickness of the samples respectively. Eq. (4) is further simplified to Eq. (5) assuming that $\frac{\theta . r}{h} \gg 1$ (Václavová et al., 2017; Xu et al., 2008; Zhilyaev et al., 2007).

$$\varepsilon = \ell n \left(\frac{2\pi N . r . h_0}{h^2} \right) \tag{5}$$

The evolution of the microhardness with strain is in this study estimated by the use of the Hollomon-Voce model proposed in (Václavová et al., 2017), which is given by the averaged curve of the Hollomon and Voce models expressed as

$$HV(\varepsilon) = \frac{1}{2} \left\{ HV_{\max}^{V} + HV_0^{H} + K . \varepsilon^m - \left(HV_{\max}^{V} - HV_0^{H} \right) \exp\left(-L . \varepsilon \right) \right\} \tag{6}$$

where $HV_0^K + K . \varepsilon^m$ is the contribution of the Hollomon model, and $HV_{\max}^{V} - \left(HV_{\max}^{V} - HV_0^{H} \right) \exp\left(-L . \varepsilon \right)$ is the Voce model. In Eq. (6), K is a material constant, m is the hardenability exponent, HV_0^H is a fitting parameter which corresponds to the microhardness of the initial unprocessed material, L is the saturation rate and $HV_{\max}^{V}$ is a fitting parameter corresponding to the saturation value of microhardness.

3. Materials and methods

3.1 Materials

The elemental composition of the Mg-SiC in this study was 91.7 Wt% of Mg, 1.4 Wt% of Silicon (Si), and 6.9 Wt% of Carbon (C). The material was supplied as 10 mm diameter rods that were sliced into disks of 1.5 mm to 2.0 mm in thicknesses. Then the disks were ground and polished to final thickness of 1.0 mm for testing. A digital vernier calliper was used to measure the thickness to ensure consistency in the thicknesses of the test specimens. The disks were then processed according to HPT with a pressure of 6.0 GPa, rotary speed of 1 rpm, at a temperature of 23 ^{0}C. This hydrostatic pressure was exerted on the samples by the top anvil of the machine while the bottom anvil exerted the torsion. The HPT process was done in an unconstrained manner which implies that quasi-material flow was permitted in the radial direction, which ensures that the required pressure was maintained without slippage due to sample shrinkage during high compression. The first disk was unprocessed with number of twist turns, N = 0; while the second through fifth disks were processed at different twist turns as follows: second disk was twisted once (N = 1), third disk was twisted five times (N = 5), and fourth disk was twisted ten times (N = 10). The processed samples were then prepared for microstructural and hardness examination.

3.2 Specimen preparation for the examination

All five specimens were prepared for this study according to the procedure outlined in the flow diagram in Fig. 1. In the figure, the produced samples of Mg-SiC were subjected to metallographic studies as well as mechanical microhardness examinations. Metallography focuses on preparing, analysing, and interpreting microstructures in engineering materials for a better understanding of materials performance and behaviour (Rosenthal et al., 2014; Wang et al., 2012). As shown in the flow diagram in Fig. **1**, the specimen undergoes grinding and polishing before microscopic examination to eliminate the machining effects that may mislead the interpretation of real microstructure of the material. Etching process was performed on the samples to ensure that Mg-SiC samples regain their mechanical properties that will be visible only under a microscope. The applied etchant was produced from the solution consisting of (150 ml) anhydrous ethyl alcohol (1 ml) of diluted glacial acetic acid and (50 ml) of distilled water (Maltais et al., 2004). Cold mounting was used to ensure that mechanical properties of Mg-SiC are not damaged or changed since it is regarded as a soft material with a melting point of 650 ^{0}C (923.15 K) and a density of 1.7 g/cm^3. Cold mounting was conducted using a mixture of epoxy resin with epofix

hardeners. Grinding and polishing were conducted using a grinding/polishing machine with the operating parameters and disk properties presented in Table 1 and Table **2**, respectively. The tables further show the desired surface finish qualitatively that was achieved for each grinding disk and polishing cloth types.

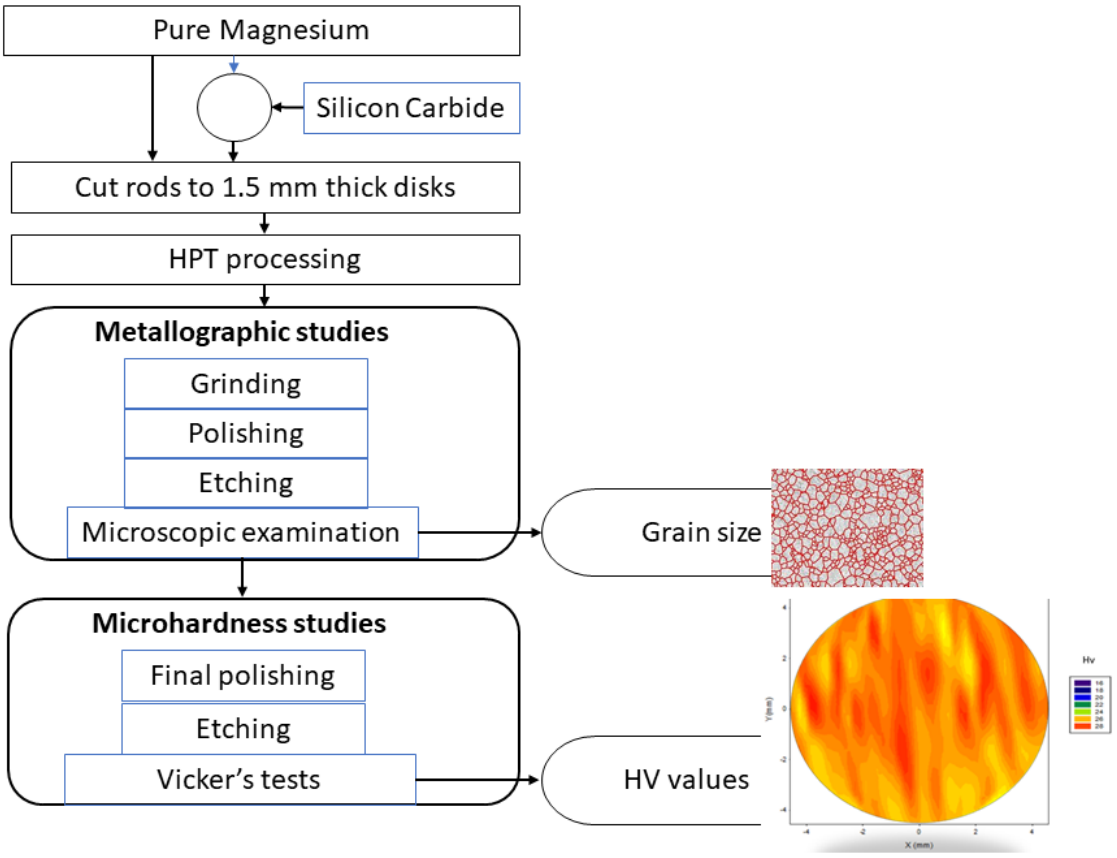

Fig. 1. The flow chart of sample preparation process for Mg-SiC including the microscopic examination and microhardness testing.

Table 1. Grinding disks, lubricant types, and machine operating parameters.

Grinding disk type	Abrasive/lubricant	Machine Load (N)	Machine Speed (rpm)	Target surface finish
Silicon Carbide foil 250 mm	Water (23^0C)	25	250	Until Plane
Silicon grinding paper	Water (23^0C)	25	150	Until Plane (smooth)

Table 2. Polishing cloth, lubricant types, and machine operating parameters.

Polishing cloth type	Abrasive/lubricant	Machine Load (N)	Machine Speed (rpm)	Target surface finish
MD-Plane 250 mm	DiaPro Plane (Dimax) 9 µm Diamond slurry	25	150	Until the sample surface is reflective
MD-Mol 200 mm	DiaPro Mol 3 µm Diamond Slurry	25	150	Until the sample surface is highly reflective
MD-Chem 200 mm	Silica (DP-Suspension P 1 µm	25	150	Until the sample surface is reflective like a mirror

For microscopic examination, the SEM was used for the visualisation of each Mg-SiC sample microstructures. For hardness examination preparation, Mg-SiC samples from the microscopic analysis were just polished according to Table 2. The mechanical hardness test was conducted using the Vickers microhardness test, which was calibrated at 50 gf (equivalent to 4.9 N) and the pressing period of 10 seconds per dent on a sample.

4. Results

4.1 Microstructural results

The characterisation of the Mg-SiC samples' microstructures in the optical microscope was performed by targeting the grain sizes for each processed sample. Fig. 2 presents the microscopic images of Mg-SiC grain sizes at different states of HPT

processing. The grains in the figure were measured by aiming at the big and small grain sizes. The resolution scale was 20 µm on all samples, which are originally indicated by the software at the lower-right hand corner of each image on the right for each frame in Fig. 2.

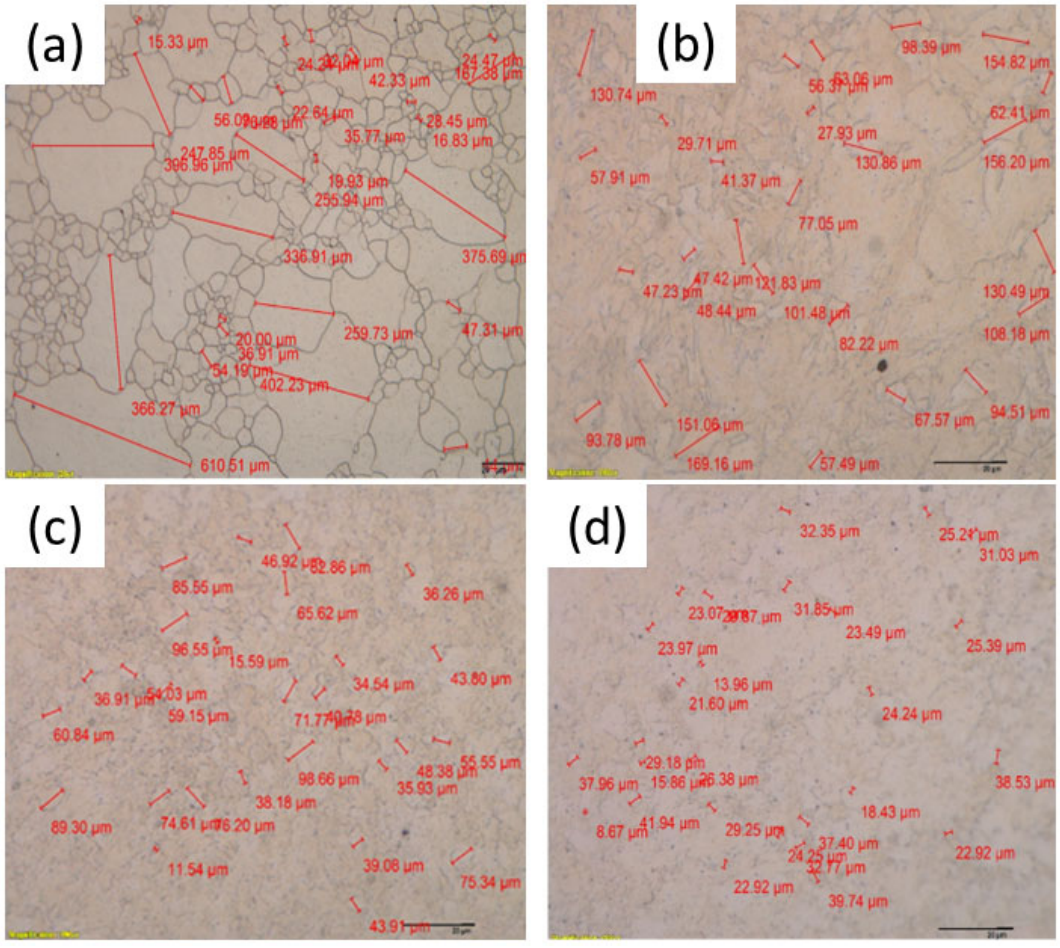

Fig. 2. Grain sizes for each number of twist turns. (a) Undeformed microstructure; (b) One twist turn; (c) Five twist turns; and (d) Ten twist turns. The images were all recorded at a scale of 20µm.

The process of measuring the Mg-SiC grain sizes was performed on each sample of Mg-SiC. The measurement of grain sizes was conducted in such a way as to measure 27 grains at each visible area of Mg-SiC under a microscope. From each measured sample, the minimum, maximum, mean, and standard deviation of the grain sizes were calculated, and are summarised in Table 3. The standard deviations of the grain sizes may be indicative of the grain size homogeneity that was attained through the HPT process across the samples. There is a marked decrease in the grain sizes from the unprocessed sample to the sample that was processed with 10 turns. This decrease in grain sizes is evident in the minimum, maximum, and average as shown in Table 3.

Table 3. Mg-SiC grain size measurement data for pure and processed samples.

Data	**N = 0**	**N = 1**	**N = 5**	**N = 10**
Minimum µm	27.93	15.33	11.54	8.67
Maximum µm	610.51	169.16	98.66	41.94
Mean µm	149.88	89.17	56.22	27.12
Percentage grain size reduction per turn	---	41%	12%	8%
Standard Deviation µm	167.07	41.96	23.34	8.06
Percentage Std Dev	111%	47%	42%	30%

However, the standard deviation shows that although there is a decrease in the spread of the grain sizes from the unprocessed samples to the samples with a higher number of turns, the decrease in the spread only takes place up to 10 turns. This might be influenced by the specific processing conditions and materials for specific HPT processes. Notice, however, the large change in both the average grain sizes and their standard deviations from the unprocessed sample to the sample that

is processed with a single turn. Actually, the percentage reduction in grain size per turn reduces from 41% for the single turn to 8% for the samples processed with 10 turns. Therefore, for the Mg-SiC under study, one may not require a large number of turns to achieve grain size refinement and homogeneity, which can be beneficial in terms of the required energy and its process efficiency. Table 3 summarises the effect of HPT number of turns on Mg-SiC grain sizes. It shows that unprocessed Mg-SiC contains large average grain sizes, and as the number of turns increases, the average grain sizes of Mg-SiC decreases. This shows that the number of processing turns is inversely proportional to the grain sizes. According to (Brandon & Kaplan, 2008; Peng et al., 2017; Tasan et al., 2015), the larger the average grain sizes of the material, the weaker the material and the smaller the average grain sizes of the material, the stronger the material. Theoretically, the strength of conventional polycrystalline materials is related to their grain size through the Hall-Petch equation given by (Lasalmonie & Strudel, 1986; Wang et al., 2012; Yu et al., 2018).

$$\sigma_Y = \sigma_0 + kd^{-1/2} \tag{6}$$

where σ_Y is the yield stress of the material, σ_0 is the lattice friction stress which for Mg-SiC is empirically determined in (Yu et al., 2018) for grain sizes of greater than 2 μm to be 124 ± 4.5 MPa, k is a material constant characterised by the stress concentration factor, and d is the grain size. It is said that the Hall-Petch relationship also applies to the flow stress and hardness dependence of the grain size for a given strain (Carsley et al., 1995; Yu et al., 2018). Thus, the average grain sizes of Mg-SiC may imply that the increase in the number of processing turns improves its strength and microhardness. In this study, we test the validity of this statement for the Mg-SiC. Only the microhardness tests were conducted in this study (owing to the practical difficulties with conducting reliable tensile tests on such smaller samples), and it was assumed that Mg-SiC obey the Tabor's relationship (Zhang et al., 2006) for the estimation of the corresponding yield strengths of the samples. Fig. 3 shows microstructural images from the VEGA3 TESCAN scanning electron microscope (SEM) with resolutions between 50 μm and 200 μm at 20 kV in high vacuum mode. The electron images show that the dispersion of the second phase within the α-phase with increased HPT turns is more uniformly distributed than in the unprocessed Mg-SiC. It was noted that substantial differences in the distribution of the second phase occurred after only one HPT processing turn at 41% grain size reduction.

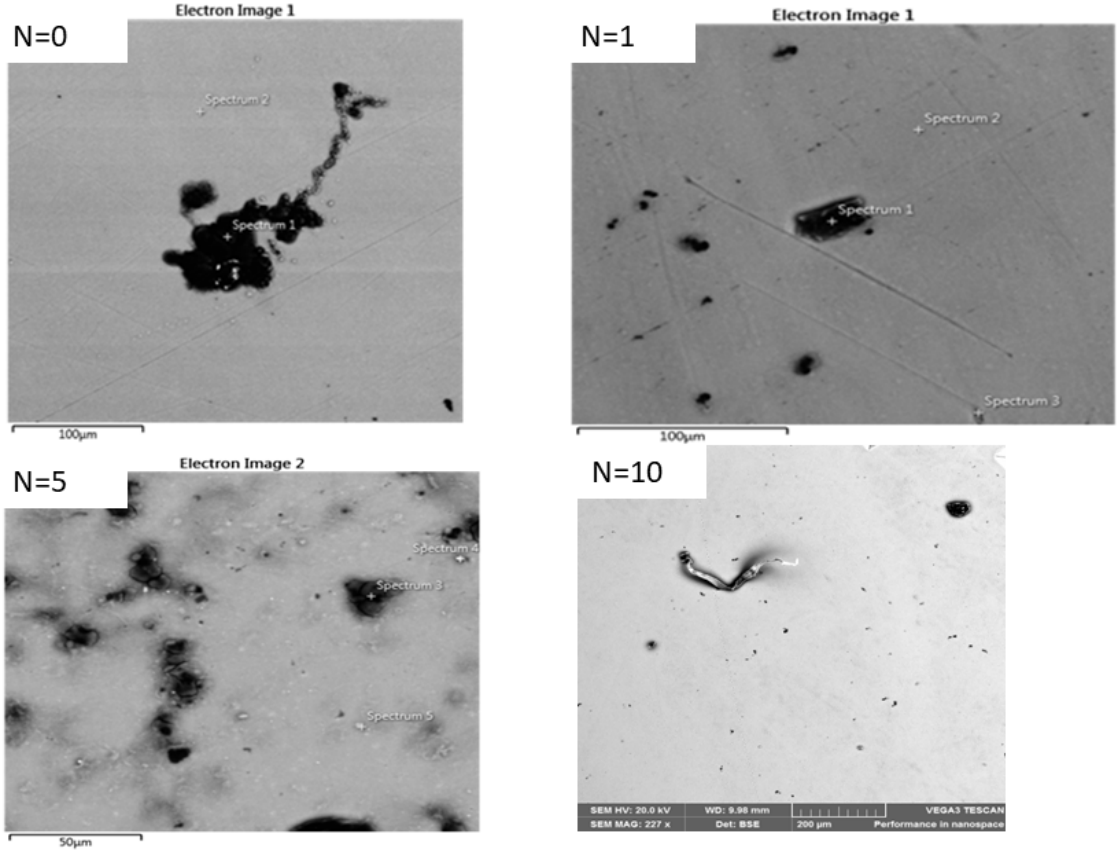

Fig. 3. Microstrustural images from the SEM showing the dispersion of precipitates within the primary phase for unprocessed specimen (N=0), one processing turn (N=1), five processing turns (N=5), and ten processing turns (N=10).

4.2 Vickers microhardness results

A microhardness test was performed on the circular cross-sectional area of each Mg-SiC sample processed by HPT according to the given number of processing turns. Since previous studies have shown that hardness values are similar on either side of the test foils (Lugo et al., 2008; Wei et al., 2006; Xu et al., 2008), in this study it did not matter which side was actually tested for microhardness testing. The results obtained during the test were recorded on an excel file so that they can be exported to sigmaPlot software to generate a contour graph as shown in Fig. **4**. The figure shows that there is a marked increase in the hardness of the tested Mg-SiC even for a single HPT processing turn. This is in agreement with previous studies that have shown that other Mg-based nanocomposites have attained substantial hardness after one-quarter of an HPT turn (Ahmadkhaniha et al., 2018; Su et al., 2018; Sun et al., 2018). For an unprocessed specimen, a large portion of the interior region exhibit high hardness values of around 24 HV which might be attributed to the effect of residual stresses induced by both sample manufacturing and sample preparation processes. As a result, these regions have attained hardness values as high as 26-28 HV after one HPT processing turn only. In fact, the proportions of the regions with hardness values ~28 HV are much larger for a single HPT processing turn than for either five or ten HPT processing turns. The processed specimens appear to have attained homogeneity after ten HPT processing turns. It is reported in (Huang et al., 2020) that hardness values evolve toward homogeneity along the disc dimeter after five and ten processing turns which seems to be the case in the currently processed Mg-SiC.

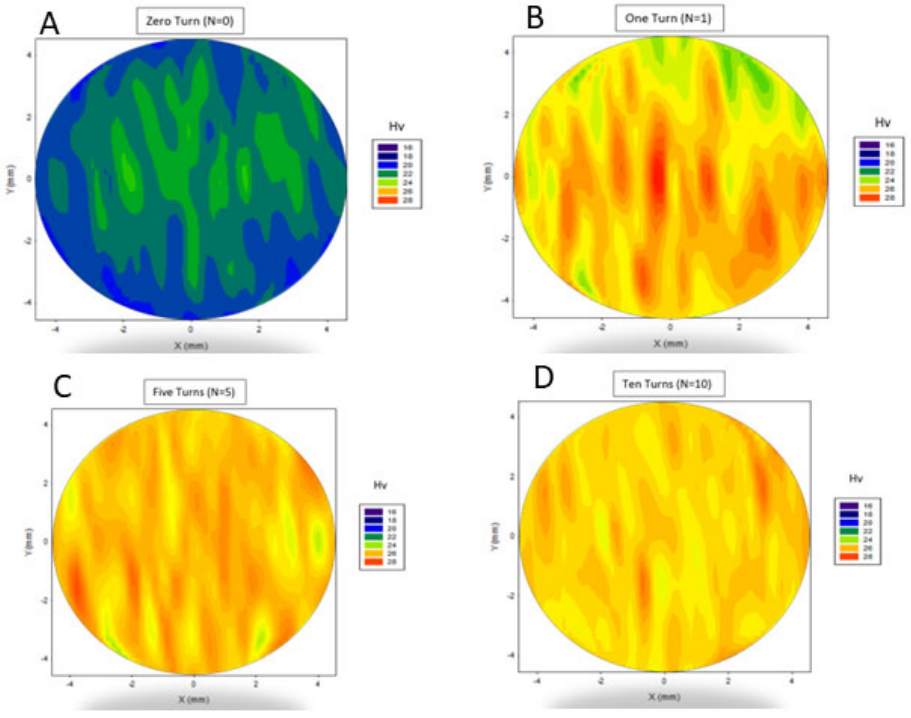

Fig. 4. Surface and contour plots showing the Vicker's hardness over the cross-sectional area of the specimen for (a) unprocessed specimen (b) one processing turn (c) 5 processing turns (d) ten processing turns.

Fig. 5 demonstrates the direct proportionality between the average hardness HV and the strain on the Mg-SiC samples. From Eq. (5) it should be clear that the strain is directly proportional to the number of HPT processing turns. This confirms that Mg-SiC gets harder as the number of HPT processing turns increases. However, the trend in the figure does not show that the increase is monotonic, apparently the curves flatten out towards higher strains, which indicates a tendency towards hardness saturation (Al-Zubaydi et al., 2016; Xu et al., 2008; Zhilyaev et al., 2007) in the HPT processed Mg-SiC. This shows that any HPT processing turns beyond 5 turns can be considered excessive especially when the gain acquired from an extra amount of hardness in the material does not warrant the amount of energy required to process the extra HPT turns. Fig. 5 also shows approximations of the microhardness values using the Hollomon model (Zener & Hollomon, 1946), Voce model, and Hollomon-Voce models (Václavová et al., 2017) as presented in Eq. (6). The results show that the Hollomon-Voce model yields the best approximations (Václavová et al., 2017). It can be observed that the increase in the microhardness values beyond one twist turn gets more diminished with higher strains at all y-ordinate positions.

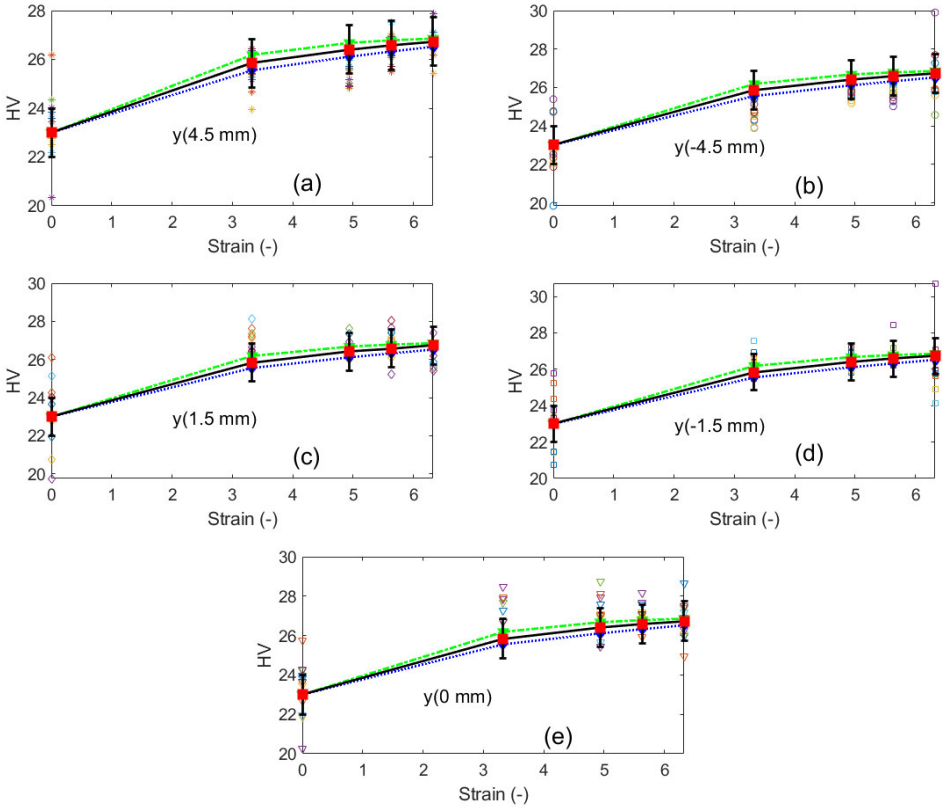

Fig. 5. Measured microhardness values plotted over Holomom, Voce, and Hollomon-Voce models' (in equation 6) prediction curves. The HV values are plotted for all the coordinate positions (at 0 mm, ± 1.5 mm, and ± 4.5 mm) against strain values calculated in Eq (5). The measured HV values are plotted as scatter points while the Hollomon and Voce model results are shown as dotted curves and the Hollomon-Voce curve is the solid darker line.

The results in Fig. 5 agree with those obtained for the grain sizes in Table 3 especially what happens towards large processing turns. The increase in the microhardness as a result of the increase in the HPT processing turns correlates with the decrease in the grain sizes of the processed material. Thus, it shows that HPT is indeed a remarkable grain refinement procedure (Edalati & Horita, 2010, 2016), and more importantly, it may not require subjecting the processed material to a large number of twist turns.

5. Discussion

The results of HPT processing of Mg-SiC show that grain sizes are refined by approximately 40% between unprocessed and single twist turn with corresponding increases in microhardness. Microhardness results plotted over a section of the surface of the specimen shows a trend towards attaining homogeneity with increased numbers of processing turns. The rate of grain refinement (per twist turn) gets diminished at higher HPT turns which implies that more work is required to achieve a given reduction in grain size at higher strains. The processed Mg-SiC follows the Hollomon-Voce model very well which demonstrates that it tends towards microhardness saturation at higher strain values corresponding to ten HPT turns.

These results are supported by statistical significance test results which show that the differences in microhardness values between unprocessed and HPT processed Mg-SiC are statistically significant. A further application of the Tukey-Kramer relationship (Hayter & Liu, 1990; Herberich et al., 2010) shows that these differences were not statistically significant between any pair of processed samples. This is irrespective of the differences in the number of twist turns. This finding is remarkable since it ensures saving in energy and cost that may be incurred by more processing turns.

Another observation is that the specimen size (thickness and diameter) under the test conditions was small enough to yield almost uniform grain sizes and microhardness values throughout its radial distance at any given number of processing turns. Larger samples at moderate hydrostatic pressures and HPT turns tend to exhibit coarser grains at the centre than around the edges hence the microhardness values at the center also tend to be lower than at the edges (Al-Zubaydi et al., 2016; Zhilyaev

et al., 2007). Other researchers (Huang et al., 2020) have however observed that HPT processed Al-0.1% Mg alloy exhibited lower hardness values at the disc edges than at its center after half, single and three turns, and that the size of the hard region in the disc center reduced as the number of turns increased from half to three turns.

The study had some limitations in that the effects of the hydrostatic pressure were not investigated. The specimen size coupled with the limitations in the testing equipment also made it hard to examine the other mechanical properties such as tensile, fatigue, and impact strength of the HPT processed material in this study.

6. Conclusions

In this study, Mg-SiC samples were processed using HPT technique at the given number of turns N = 0, N = 1, N = 5, and N =10 under a constant hydrostatic pressure of 6 GPa. The samples were further prepared for microstructural characterisation and the Vickers microhardness testing. Besides the widely publicised results that HPT improves grain size refinement, strength and hardness of the processed specimens, this study shows that the rate of reduction in the grain sizes within the processed samples actually decreases with increased twist turns thereby driving the microhardness of the sample into saturation. Under the test conditions in this study, the grain size reduction per turn decreased from 41% reduction for a single turn to 8% reduction for ten turns. The study further shows that microhardness homogeneity across the specimen's cross-section progressively improves with increased number of twist turns. The SEM microstructural results also show the uniform distribution of the fine grains of the precipitates within the matrix with increased numbers of HPT processing turns. This uniform distribution of secondary phase within the matrix might hinder grain growth (Carvalho & Figueiredo, 2022) which implies further enhances grain size reduction. However, this study did not investigate the effects of changes in the applied hydrostatic pressure, rotational speed during torsion and the temperature, corrosion resistance as well as other mechanical properties such as tensile, fatigue, creep, and impact strength. It would be interesting to find out the effects of these operating conditions to the rate of grain size reduction, microhardness, and sample homogeneity across the cross-section. Other studies (Abyzov et al., 2015; Gubicza, 2020; Gubicza et al., 2020; Khaleghi et al., 2021) have shown that changes in precipitates and dislocation density correlate with hardness in the HPT processed specimens, which have also not been investigated in this particular study.

Statements and Declarations

Competing interests: All authors certify that they have no affiliations with or involvement in any organization or entity with any financial interest or non-financial interest in the subject matter or materials discussed in this manuscript.

Financial interests: The authors received support from the Rural Education Access Programme (REAP) of South Africa for the research.

Non-finacial interests: none.

Author Contributions

All authors contributed to the study conception and design. Material preparation and data collection were performed by Ronny T Tebeta, Data analysis were performed by Harry M Ngwangwa and Ronny T Tebeta. The first draft of the manuscript was written by Ronny T Tebeta. Harry M Ngwangwa, Nkosinathi Madushele, Daniel M Madyira and Zongshen Wang revised the original manuscript to the current version. All authors read and approved the final manuscript.

- Conceptualization: RT Tebeta, Methodology: RT Tebeta and Daniel M Maadyira; Formal analysis and investigation: RT Tebeta and HM Ngwangwa; Writing – original draft preparation: RT Tebeta; Editing: HM Ngwangwa, N Madushele, D.M. Madyira and Z. Wang; Resources: N Madushele and D.M. Madyira; Supervision: D.M. Madyira and H.M. Ngwangwa

Acknowledgments

The authors are grateful to the Rural Education Access Programme (REAP) of South Africa, Prof N.A. Ahmed and Prof A.M. Fattahi. The authors are also very grateful to the assistane rendered by the English editor Malvin Vergie at the University of South Africa.

References

Abyzov, A. M., Shakhov, F. M., Averkin, A. I., & Nikolaev, V. I. (2015). Mechanical properties of a diamond-copper composite with high thermal conductivity. *Materials and Design*, *87*, 527–539. https://doi.org/10.1016/j.matdes.2015.08.048

Ahmadkhaniha, D., Huang, Y., Jaskari, M., Järvenpää, A., Sohi, M. H., Zanella, C., Karjalainen, L. P., & Langdon, T. G. (2018). Effect of high-pressure torsion on microstructure, mechanical properties and corrosion resistance of cast pure Mg. *Journal of Materials Science*, *53*(24), 16585–16597. https://doi.org/10.1007/s10853-018-2779-1

Al-Zubaydi, A. S. J., Zhilyaev, A. P., Wang, S. C., Kucita, P., & Reed, P. A. S. (2016). Evolution of microstructure in AZ91 alloy processed by high-pressure torsion. *Journal of Materials Science*, *51*(7), 3380–3389. https://doi.org/10.1007/s10853-015-9652-2

Alil, A., Popovic', M., Radetic', T., & Romhanji, E. (2014). Influence of an accummulative roll bonding (ARB) process on the properties of AA5083 Al-Mg alloy sheets. *Metallurgical and Materials Engineering*, *20*(4), 285–295.

Alsubaie, S. A., Bazarnik, P., Huang, Y., Lewandowska, M., & Langdon, T. G. (2022). Achieving superplastic elongations in an AZ80 magnesium alloy processed by high-pressure torsion. *Advanced Engineering Materials*, *2200620*. https://doi.org/10.1002/adem.202200620

Alsubaie, S. A., Bazarnik, P., Lewandowska, M., Huang, Y., & Langdon, T. G. (2016). Evolution of microstructure and hardness in an AZ80 magnesium alloy processed by high-pressure torsion. *Journal of Materials Research and Technology*, *5*(2), 152–158. https://doi.org/10.1016/j.jmrt.2015.11.006

Brandon, D., & Kaplan, W. D. (2008). *Microstructural characterization of materials* (2nd Editio). John Wiley & Sons, Ltd. https://doi.org/10.1002/9780470727133

Brunner, P., Brumbauer, F., Steyskal, E.-M., Renk, O., Weinberg, A.-M., Schroettner, H., & Wurschum, R. (2021). Influence of high-pressure torsion deformation on the corrosion behaviour of bioresorbable Mg-based allow studied by positron annihilation. *Biomaterials Science*, *9*, 4099–4109.

Carsley, J. E., Ning, J., Milligan, W. W., Hackney, S. A., & Aifantis, E. C. (1995). A simple, mixtures-based model for the grain size dependence of strength in nanophase metals. *Nanostructured Materials*, *5*(4), 441–448. https://doi.org/10.1016/0965-9773(95)00257-F

Carvalho, A. P., & Figueiredo, R. B. (2022). The effect of ultragrain refinement on the strength and strain rate sensitivity of a ZK60 Magnesium alloy. *Advanced Engineering Materials*, *24*(3), 1–7. https://doi.org/10.1002/adem.202100846

Dziubińska, A., Gontarz, A., Dziubiński, M., & Barszcz, M. (2016). The forming of Magnesium alloy forgings for aircraft and automotive applications. *Advances in Science and Technology Research Journal*, *10*(31), 158–168. https://doi.org/10.12913/22998624/64003

Edalati, K., & Horita, Z. (2010). Continuous high-pressure torsion. *Journal of Materials Science*, *45*(17), 4578–4582. https://doi.org/10.1007/s10853-010-4381-z

Edalati, K., & Horita, Z. (2016). A review on high-pressure torsion (HPT) from 1935 to 1988. *Materials Science and Engineering A*, *652*, 325–352. https://doi.org/10.1016/j.msea.2015.11.074

Figueiredo, R. B., & Langdon, T. G. (2019). Processing Magnesium and its alloys by high-pressure torsion: An overview. *Advanced Engineering Materials*, *21*(1), 1–15. https://doi.org/10.1002/adem.201801039

Gubicza, J. (2020). Annealing-induced hardening in ultrafine-grained and nanocrystalline materials. *Advanced Engineering Materials*, *22*(1). https://doi.org/10.1002/adem.201900507

Gubicza, J., El-Tahawy, M., Lábár, J. L., Bobruk, E. V., Murashkin, M. Y., Valiev, R. Z., & Chinh, N. Q. (2020). Evolution of microstructure and hardness during artificial aging of an ultrafine-grained Al-Zn-Mg-Zr alloy processed by high pressure torsion. *Journal of Materials Science*, *55*(35), 16791–16805. https://doi.org/10.1007/s10853-020-05264-4

Gupta, M., & Sharon, N. M. L. (2011). Magnesium, Magnesium alloys, and Magnesium composites. In *John Wiley & Sons, Inc*. https://doi.org/10.1007/978-3-319-69743-7_5

Harai, Y., Kai, M., Kaneko, K., Horita, Z., & Langdon, T. G. (2008). Microstructural and mechanical characteristics of AZ61 Magnesium alloy processed by high-pressure torsion. *Materials Transactions*, *49*(1), 76–83. https://doi.org/10.2320/matertrans.ME200718

Hayter, A., & Liu, W. (1990). The power function of the studentised range test. *The Annals of Statistics*, *18*(1), 465–468.

Herberich, E., Sikorski, J., & Hothorn, T. (2010). A robust procedure for comapring multiple means under heteroscedasticity in unbalanced designs. *PLoS ONE*, *5*(3), e9788. https://doi.org/10.1371/journal.pone.0009788

Holweg, P., Berger, L., Cihova, M., Donohue, N., Clement, B., Schwarze, U., Sommer, N. G., Hohenberger, G., van den Beucken, J. J. J. P., Seibert, F., Leithner, A., Löffler, J. F., & Weinberg, A. M. (2020). A lean magnesium–zinc–calcium alloy ZX00 used for bone fracture stabilization in a large growing-animal model. *Acta Biomaterialia*, *113*, 646–659. https://doi.org/10.1016/j.actbio.2020.06.013

Huang, Y., Millet, J., Zhang, N. X., Jenei, P., Gubicza, J., & Langdon, T. G. (2020). An investigation of strain-softening phenomenon in Al–0.1% Mg alloy during high-pressure torsion processing. *Advanced Engineering Materials*, *22*(10), 1–7. https://doi.org/10.1002/adem.201901578

Ibrahim, H., Klarner, A. D., Poorganji, B., Dean, D., Luo, A. A., & Elahinia, M. (2017). Microstructural, mechanical and corrosion characteristics of heat-treated Mg-1.2Zn-0.5Ca (wt%) alloy for use as resorbable bone fixation material. *Journal of the Mechanical Behavior of Biomedical Materials*, *69*(December 2016), 203–212. https://doi.org/10.1016/j.jmbbm.2017.01.005

Khaleghi, A. A., Akbaripanah, F., Sabbaghian, M., Máthis, K., Minárik, P., Veselý, J., El-Tahawy, M., & Gubicza, J. (2021). Influence of high-pressure torsion on microstructure, hardness and shear strength of AM60 magnesium alloy. *Materials Science and Engineering A*, *799*(August 2020). https://doi.org/10.1016/j.msea.2020.140158

Lasalmonie, A., & Strudel, J. L. (1986). Influence of grain size on the mechanical behaviour of some high strength materials. *Journal of Materials Science*, *21*(6), 1837–1852. https://doi.org/10.1007/BF00547918

Lugo, N., Llorca, N., Cabrera, J. M., & Horita, Z. (2008). Microstructures and mechanical properties of pure copper deformed severely by equal-channel angular pressing and high pressure torsion. *Materials Science and Engineering: A*, *477*(1–2), 366–371. https://doi.org/10.1016/j.msea.2007.05.083

Maltais, A., Dubé, D., Fiset, M., Laroche, G., & Turgeon, S. (2004). Improvements in the metallography of as-cast AZ91 alloy. *Materials Characterization*, *52*(2), 103–119. https://doi.org/10.1016/j.matchar.2004.04.002

Mizelli-Ojdanic, A., Horky, J., Mingler, B., Fanetti, M., Gardonio, S., Valant, M., Sulkowski, B., Schafler, E., Orlov, D., & Zehetbauer, M. J. (2021). Enhancing the mechanical properties of biodegradable mg alloys processed by warm HPT and thermal treatments. *Materials*, *14*(21). https://doi.org/10.3390/ma14216399

Peng, J., Wong, L. N. Y., & Teh, C. I. (2017). Influence of grain size heterogeneity on strength and microcracking behavior of crystalline rocks. *Journal of Geophysical Research: Solid Earth*, *122*(2), 1054–1073. https://doi.org/10.1002/2016JB013469

Rosalie, J. M., & Pauw, B. R. (2014). Form-free size distributions from complementary stereological TEM/SAXS on precipitates in a Mg-Zn alloy. *Acta Materialia*, *66*, 150–162. https://doi.org/10.1016/j.actamat.2013.11.029

Rosenthal, I., Stern, A., & Frage, N. (2014). Microstructure and mechanical properties of AlSi10Mg parts produced by the laser beam additive manufacturing (AM) technology. *Metallography, Microstructure, and Analysis*, *3*(6), 448–453. https://doi.org/10.1007/s13632-014-0168-y

Ross, R. B. (2013). *Metallic materials specification handbook* (4th Editio). Springer Science & Business Media. https://doi.org/10.1007/978-1-4615-3482-2

Shirooyeh, M., Xu, J., & Langdon, T. G. (2014). Microhardness evolution and mechanical characteristics of commercial purity titanium processed by high-pressure torsion. *Materials Science and Engineering A*, *614*, 223–231. https://doi.org/10.1016/j.msea.2014.07.030

Su, Q., Xu, J., Li, Y., Yoon, J. I., Shan, D., Guo, B., & Kim, H. S. (2018). Microstructural evolution and mechanical properties in superlight Mg-Li alloy processed by high-pressure torsion. *Materials*, *11*(4). https://doi.org/10.3390/ma11040598

Sun, W. T., Qiao, X. G., Zheng, M. Y., He, Y., Hu, N., Xu, C., Gao, N., & Starink, M. J. (2018). Exceptional grain refinement in a Mg alloy during high pressure torsion due to rare earth containing nanosized precipitates. *Materials Science and Engineering A*, *728*(May), 115–123. https://doi.org/10.1016/j.msea.2018.05.021

Tasan, C. C., Diehl, M., Yan, D., Bechtold, M., Roters, F., Schemmann, L., Zheng, C., Peranio, N., Ponge, D., Koyama, M., Tsuzaki, K., & Raabe, D. (2015). An overview of dual-phase steels: Advances in microstructure-oriented processing and micromechanically guided design. *Annual Review of Materials Research*, *45*, 391–431. https://doi.org/10.1146/annurev-matsci-070214-021103

Václavová, K., Stráský, J., Polyakova, V., Stráská, J., Nejezchlebová, J., Seiner, H., Semenova, I., & Janeček, M. (2017). Microhardness and microstructure evolution of ultra-fine grained Ti-15Mo and TIMETAL LCB alloys prepared by high pressure torsion. *Materials Science and Engineering A*, *682*(November 2016), 220–228. https://doi.org/10.1016/j.msea.2016.11.038

Valiev, R. Z., Islamgaliev, R. K., & Alexandrov, I. V. (2000). Bulk nanostructured materials from severe plastic deformation. In *Progress in Materials Science* (Vol. 45, Issue 2). https://doi.org/10.1016/S0079-6425(99)00007-9

Wang, M. Y., Xu, Y. J., Jing, T., Peng, G. Y., Fu, Y. N., & Chawla, N. (2012). Growth orientations and morphologies of α-Mg dendrites in Mg-Zn alloys. *Scripta Materialia*, *67*(7–8), 629–632. https://doi.org/10.1016/j.scriptamat.2012.07.031

Wei, Q., Zhang, H. T., Schuster, B. E., Ramesh, K. T., Valiev, R. Z., Kecskes, L. J., Dowding, R. J., Magness, L., & Cho, K. (2006). Microstructure and mechanical properties of super-strong nanocrystalline tungsten processed by high-pressure torsion. *Acta Materialia*, *54*(15), 4079–4089. https://doi.org/10.1016/j.actamat.2006.05.005

Xu, C., Horita, Z., & Langdon, T. G. (2008). The evolution of homogeneity in an aluminum alloy processed using high-pressure torsion. *Acta Materialia*, *56*(18), 5168–5176. https://doi.org/10.1016/j.actamat.2008.06.036

Yu, H., Xin, Y., Wang, M., & Liu, Q. (2018). Hall-Petch relationship in Mg alloys: A review. *Journal of Materials Science and Technology*, *34*(2), 248–256. https://doi.org/10.1016/j.jmst.2017.07.022

Zener, C., & Hollomon, J. (1946). Problems in non-elastic deformation. *Journal of Applied Physics*, *17*(2), 69–82. https://doi.org/https://doi.org/10.1063/1.1707696

Zhang, H. W., Subhash, G., Jing, X. N., Kecskes, L. J., & Dowding, R. J. (2006). Evaluation of hardness-yield strength relationships for bulk metallic glasses. *Philosophical Magazine Letters*, *86*(5), 333–345. https://doi.org/10.1080/09500830600788935

Zhilyaev, A. P., & Langdon, T. G. (2008). Using high-pressure torsion for metal processing: Fundamentals and applications. *Progress in Materials Science*, *53*(6), 893–979. https://doi.org/10.1016/j.pmatsci.2008.03.002

Zhilyaev, A. P., McNelley, T. R., & Langdon, T. G. (2007). Evolution of microstructure and microtexture in fcc metals during high-pressure torsion. *Journal of Materials Science*, *42*(5), 1517–1528. https://doi.org/10.1007/s10853-006-0628-0

Zhu, Y. T., Lowe, T. C., & Langdon, T. G. (2004). Performance and applications of nanostructured materials produced by severe plastic deformation. *Scripta Materialia*, *51*(8 SPEC. ISS.), 825–830. https://doi.org/10.1016/j.scriptamat.2004.05.006